JACS ARTICLES

Published on Web 10/05/2010

Effect of Morphology on Ultrafast Free Carrier Generation in Polythiophene:Fullerene Organic Solar Cells

Ian A. Howard,* Ralf Mauer, Michael Meister, and Frédéric Laquai*

Max Planck Research Group for Organic Optoelectronics, Max Planck Institute for Polymer Research, Ackermannweg 10, D-55128 Mainz, Germany

Received June 16, 2010; E-mail: ian.howard@mpip-mainz.mpg.de; laquai@mpip-mainz.mpg.de

Abstract: Despite significant study, the precise mechanisms that dictate the efficiency of organic photovoltaic cells, such as charge separation and recombination, are still debated. Here, we directly observe efficient ultrafast free charge generation in the absence of field in annealed poly(3-hexylthiophene):methanofullerene (P3HT:PCBM). However, we find this process is much less efficient in unannealed and amorphous regiorandom blends, explaining the superior short-circuit current and fill-factor of annealed RR-P3HT:PCBM solar cells. We use transient optical spectroscopy in the visible and near-infrared spectral region covering, but not limited to, the previously unobserved and highly relevant time scale spanning 1 to 100 ns, to directly observe both geminate and nongeminate charge recombination. We find that exciton quenching leads directly (time scale less than 100 fs) to two populations: bound charges and free charges. The former do not lead to photocurrent in a photovoltaic cell; they recombine geminately within 2 ns and are a loss channel. However, the latter can be efficiently extracted in photovoltaic cells. Therefore, we find that the probability of ultrafast free charge formation after exciton quenching directly limits solar cell efficiency. This probability is low in disordered P3HT:PCBM blends but approaches unity in annealed blends.

1. Introduction

Organic photovoltaic cells (OPVs) are based on partially demixed blends of electron-donating and electron-accepting materials. They have the advantage over their inorganic counterparts of the potential for low-cost, large-area fabrication and have reached power conversion efficiencies of over 7%.[1] The efficiency with which they convert sunlight into electrical power depends on the product of two factors: their quantum efficiency (current generated per photon absorbed) and their energy efficiency (fraction of photon energy retained by an extracted charge). The quantum efficiency itself is determined by the product of the efficiencies of a cascade of events: photon absorption, exciton quenching, charge separation, and charge extraction. These events occur over highly disparate time and length scales. Although various methods of altering the morphology, from thermal and solvent-vapor annealing,[2,3] to deposition from solvent mixtures,[4,5] have been used to optimize the quantum efficiency in many OPV blends, the complexity and widely ranging time and length scales of the quantum efficiency cascade mean that firm understanding of the precise structure−function relationship is still developing.

Recently, detailed morphological and time-resolved optical studies have begun to clarify this structure−function relationship. Direct observation with sub-10 nm resolution of the blend morphology over 100 nm thickness and a micrometer size area has recently been achieved for the benchmark P3HT:PCBM blends using electron tomography, with the key finding that annealing develops ordered P3HT nanorods with widths around 15 nm, thicknesses of a few nanometers, and lengths on the scale of micrometers.[6] Furthermore, Ohkita et al. recently demonstrated that the annealing and order in the P3HT phase strongly enhances the generation of separated charges and suppresses loss during carrier collection.[7] By extending the observation of charge recombination to cover its entire progress (200 fs to 10 μs), including the previously unobserved but critically relevant intermediate time scale of 3−100 ns, we gain physical insight into how the transition from amorphous to better ordered P3HT domains affects both the generation of free charges and their recombination. We directly observe that annealing of P3HT:PCBM blends leads to ultrafast free charge generation. This prompt generation process is inconsistent with theoretical models based on an Onsager−Braun type charge separation through a Coulombically bound pair and elucidates why parameters for the charge-pair lifetimes in such models had to exceed experimentally observed values by several orders of magnitude.[8] Our work therefore highlights not only the critical role of local order in the high quantum efficiency of P3HT:

(1) Liang, Y.; Xu, Z.; Xia, J.; Tsai, S.-T.; Wu, Y.; Li, G.; Ray, C.; Yu, L. *Adv. Mater.* **2010**, *xx*, in press.
(2) Padinger, F.; Rittberger, R. S.; Sariciftci, N. S. *Adv. Funct. Mater.* **2003**, *13*, 85.
(3) Li, G.; Yao, Y.; Yang, H.; Shrotriya, V.; Yang, G.; Yang, Y. *Adv. Funct. Mater.* **2007**, *17*, 1636.
(4) Zhang, F.; Jespersen, K. G.; Björström, C.; Svensson, M.; Andersson, M. R.; Sundström, V.; Magnusson, K.; Moons, E.; Yartsev, A.; Inganäs, O. *Adv. Funct. Mater.* **2006**, *16*, 667.
(5) Campbell, A. R.; Hodgkiss, J. M.; Westenhoff, S.; Howard, I. A.; Marsh, R. A.; McNeill, C. R.; Friend, R. H.; Greenham, N. C. *Nano Lett.* **2008**, *8*, 3942.
(6) Van Bavel, S. S.; Sourty, E.; De With, G.; Loos, J. *Nano Lett.* **2009**, *9*, 507.
(7) Guo, J. M.; Ohkita, H.; Benten, H.; Ito, S. *J. Am. Chem. Soc.* **2010**, *132*, 6154.
(8) Deibel, C.; Strobel, T.; Dyakonov, V. *Phys. Rev. Lett.* **2009**, *103*, 036402.

10.1021/ja105260d

PCBM solar cells but also the need to develop a better theoretical understanding, perhaps encompassing correlated disorder,[9] of charge separation at junctions between organic semiconductors.

As model systems we use regiorandom (RRa) P3HT and highly (>98%) regioregular (RR) P3HT (BASF Sepiolid P200) blended with PCBM. Transient changes of the excited state absorption of pristine polymers as well as blends are monitored in the visible and in the near-infrared spectral region (500−1100 nm), and spectra are compared with those obtained by quasi-steady-state photoinduced absorption spectroscopy. This allows us to clearly assign the contribution of the individual excited states to the absorption spectra that we observe and also assemble in a stepwise fashion a clear and quantitative understanding of the population transitions.

2. Models of Charge Separation and Recombination

Before presenting our experimental results, we briefly outline two theoretical frameworks for considering the quantum efficiency loss mechanisms in organic solar cells that we will later compare with our data. However, first we briefly discuss the charge recombination reactions that play a role in these models.

2.1. Monomolecular and Bimolecular Charge Recombination. A first important distinction between loss mechanisms in organic solar cells is whether they follow monomolecular or bimolecular kinetics. Monomolecular processes occur with the same rate (and probability) irrespective of the illumination intensity, while bimolecular processes occur more quickly at higher excited state densities created by more intense illumination. Therefore, monomolecular processes cause a fixed loss of quantum efficiency at all intensities, while bimolecular processes cause a variable loss that becomes more severe at higher illumination.

When an electron and hole generated by the quenching of a single exciton recombine with one another it is termed geminate recombination.[10−12] Geminate recombination may repopulate the ground state, or, in high open-circuit voltage blends, populate an energetically accessible triplet exciton state.[12,13] In either case, it is a monomolecular terminal loss mechanism and reduces the quantum efficiency by a fixed factor at all illumination intensities.

When two free opposite charges recombine it is called nongeminate recombination. The rate of nongeminate recombination depends on the density of the spatially separated (or free) charges, and therefore the rate of nongeminate recombination depends on the intensity of the light excitation. In previous investigations of P3HT:PCBM blends, the nongeminate recombination rate was usually observed to have an order greater than 2 (which is the order theoretically expected for 3D Langevin recombination).[14−16] This stronger dependence on charge density could imply that the mobility depends on charge density,[17,18] the morphology restricts the dimensionality of charge diffusion,[19] a trap density alters recombination dynamics,[20] or a combination of these factors. In any case, the amount of loss this type of recombination causes depends on the illumination intensity. In P3HT:PCBM solar cells at short circuit conditions under solar illumination intensity, nongeminate recombination is so low as to be negligible.[18,21]

When one free carrier is caught in an immobile trap state and then subsequently recombines with another free carrier it is called trap-assisted recombination. Depending on whether or not the trap density can be approximated as constant, trap-assisted recombination can follow density-dependent or -independent kinetics.

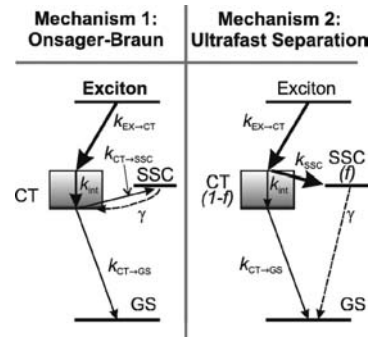

Figure 1. Illustrations of the two limiting cases for the mechanism of charge generation and separation. CT stands for charge-transfer state, SSC for spatially separated (free) charges, and GS for ground state. In mechanism 1 the thermal relaxation of the charge-transfer state is much faster than separation; consequently charge separation and recombination are mediated by the relaxed charge-transfer state. An Onsager−Braun type description of charge separation should be applicable and separation times of certainly >1 ns are expected. In the second limiting case, the spatial separation of charges in hot charge-transfer states created directly after exciton quenching rivals or exceeds the rate of internal conversion in the CT manifold. In this case, free, spatially separated charges are generated on a very fast time scale (<100 fs). See text for further details.

2.2. Onsager−Braun Charge Separation. Two limiting cases for the mechanism of charge generation and recombination can be considered.[22,23] These are schematically illustrated in Figure 1. The first mechanism, like the Onsager−Braun model, considers that charge separation occurs in kinetic competition with recombination from an equilibrated geminate pair. In this mechanism a hot charge-transfer state created by exciton quenching first quickly relaxes (∼100 fs time scale) to its lowest excited electronic and vibrational level. Thereafter, on a longer ∼5 ns time scale, the charges held in such relaxed charge-

(9) Groves, C.; Blakesley, J. C.; Greenham, N. C. *Nano Lett.* **2010**, *10*, 1063.
(10) Clarke, T.; Ballantyne, A.; Jamieson, F.; Brabec, C.; Nelson, J.; Durrant, J. *Chem. Commun.* **2009**, 89.
(11) De, S.; Pascher, T.; Maiti, M.; Jespersen, K. G.; Kesti, T.; Zhang, F. L.; Inganas, O.; Yartsev, A.; Sundstrom, V. *J. Am. Chem. Soc.* **2007**, *129*, 8466.
(12) Westenhoff, S.; Howard, I. A.; Hodgkiss, J. M.; Kirov, K. R.; Bronstein, H. A.; Williams, C. K.; Greenham, N. C.; Friend, R. H. *J. Am. Chem. Soc.* **2008**, *130*, 13653.
(13) Ohkita, H.; Cook, S.; Astuti, Y.; Duffy, W.; Heeney, M.; Tierney, S.; McCulloch, I.; Bradley, D. D. C.; Durrant, J. R. *Chem. Commun.* **2006**, 3939.
(14) Shuttle, C. G.; O'Regan, B.; Ballantyne, A. M.; Nelson, J.; Bradley, D. D. C.; Durrant, J. R. *Phys. Rev. B* **2008**, *78*, 113201.
(15) Shuttle, C. G.; O'Regan, B.; Ballantyne, A. M.; Nelson, J.; Bradley, D. D. C.; de Mello, J.; Durrant, J. R. *Appl. Phys. Lett.* **2008**, *92*, 093311.
(16) Clarke, T. M.; Jamieson, F. C.; Durrant, J. R. *J. Phys. Chem. C* **2009**, *113*, 20934.
(17) Pasveer, W. F.; Cottaar, J.; Tanase, C.; Coehoorn, R.; Bobbert, P. A.; Blom, P. W. M.; de Leeuw, D. M.; Michels, M. A. J. *Phys. Rev. Lett.* **2005**, *94*, 206601.
(18) Shuttle, C. G.; Hamilton, R.; Nelson, J.; O'Regan, B. C.; Durrant, J. R. *Adv. Funct. Mater.* **2010**, *20*, 698.
(19) Juska, G.; Genevicius, K.; Nekrasas, N.; Sliauzys, G.; Osterbacka, R. *Appl. Phys. Lett.* **2009**, *95*, 013303.
(20) Nelson, J.; Choulis, S. A.; Durrant, J. R. *Thin Solid Films* **2004**, *451−452*, 508.
(21) Marsh, R. A.; McNeill, C. R.; Abrusci, A.; Campbell, A. R.; Friend, R. H. *Nano Lett.* **2008**, *8*, 1393.
(22) Brédas, J. L.; Norton, J. E.; Cornil, J.; Coropceanu, V. *Acc. Chem. Res.* **2009**, *42*, 1691.
(23) Clarke, T. M.; Durrant, J. R. *Chem. Rev.* **2010** *xx*, in press.

transfer states hop, either to become spatially separated (a process that is endothermic or at least goes through a higher energy intermediate because the charge-transfer state still has a significant binding energy),[22] or to come into such close proximity that they recombine geminately. A key feature of this first mechanism is that the rate (and therefore also yield) of carrier separation is increased by the drift of charges caused by the electric field inside the device. This means that as the field in the device increases, the charge-transfer states separate more quickly and therefore their lifetime and luminescence decreases, while at the same time the quantum efficiency of the device increases.[24] In a blend in which the charge-transfer state is emissive, the charge-transfer state lifetime can be directly monitored by temporally resolving its emission. This method has been used to show that the charge-transfer state lifetime in fluorene:PCBM OPVs does indeed decrease with increasing field,[25] showing the relevance of the Onsager−Braun type mechanism of charge separation. Also in P3HT:PCBM solar cells, wherein CT emission is difficult to temporally resolve, recent bias-dependent transient absorption measurements,[26] and correlation of the above- and below-bandgap absorption and photocurrent,[27] are interpreted to support this mechanism of charge generation, with the latter also suggesting excess energy does not increase the probability of charge separation. Also, Monte Carlo simulations based on these assumptions have provided reasonable descriptions of the morphological effects of blend structure on charge separation.[28] However, the support for this model is by no means universal. Neher and co-workers have recently demonstrated that charge-transfer state separation cannot account for all of the photocurrent observed, and that at low fields the photocurrent must come from a different source.[29] Futhermore, in order to explain the field dependence of photocurrent using such a model, exceedingly long charge-transfer state lifetimes ($\sim$7 μs) that are inconsistent with experimental observations ($\sim$10 ns) must be used.[24]

The rate equations that describe the population evolutions in this mechanism are shown in eq 1, wherein CT is the charge-transfer state population, SSC is the spatially separated electron population, GS is the population returned to the ground state, $k_{i\rightarrow j}$ is a characteristic rate for monomolecular flow from population i to population j, γ is the density-dependent recombination rate constant, and $\lambda + 1$is the order of the density-dependent ("bimolecular") recombination. For 3D isotropic Langevin recombination with a time and carrier-density independent mobility $\lambda = 1$, as mentioned earlier λ can exceed 1 if the morphology limits the dimensionality of diffusion or the charge mobility is time- or density-dependent. In this first mechanism, the fraction of geminate recombination is given by $k_{CT\rightarrow GS}/(k_{CT\rightarrow GS} + k_{CT\rightarrow SSC})$, the total depletion rate of the initially formed charge-transfer states is $k_{tot} = k_{CT\rightarrow SSC} + k_{CT\rightarrow GS}$, the fraction of nongeminate recombination is $k_{CT\rightarrow SSC}/(k_{CT\rightarrow GS} + k_{CT\rightarrow SSC})$, and the effective rate of nongeminate recombination is $\gamma k_{CT\rightarrow GS}/(k_{CT\rightarrow GS} + k_{CT\rightarrow SSC})$. Here we see that when separation is much more likely than recombination ($k_{CT\rightarrow SSC} > > k_{CT\rightarrow GS}$), the effective bimolecular recombination rate will be strongly reduced, which would be consistent with the experimentally observed bimolecular recombination rates being much lower than that predicted by the Langevin equation.[30] To summarize, in this mechanism the charge-transfer state is a key intermediate state, with the rate of separation versus recombination determining the amount of geminate vs nongeminate recombination and also mediating the rate of the bimolecular recombination.

$$\begin{aligned} dCT/dt &= -k_{CT\rightarrow GS}CT - k_{CT\rightarrow SSC}CT + \gamma SSC^{\lambda+1} \\ dSSC/dt &= k_{CT\rightarrow SSC}CT - \gamma SSC^{\lambda+1} \\ dGS/dt &= k_{CT\rightarrow GS}CT \end{aligned} \quad (1)$$

2.3. Ultrafast Charge Separation. The second mechanism involves direct spatial separation of charges from excited ('hot') charge-transfer states before they thermally relax and predicts different yields and kinetics for geminate and nongeminate recombination compared to the Onsager−Braun model. The precise mechanism for the charge separation is still unclear; it is proposed that the excess energy of the strongly exothermic exciton quenching can be directly translated into kinetic energy of the electron and hole[31] or that, similar to charge formation from highly excited singlet excitons in a pristine material, a greater separation of electron and hole in the wave function of higher excited CT states leads directly to separated charges.[22] Nonetheless, the key feature of this mechanism is that on an ultrafast time scale after exciton quenching either free charges or a thermally relaxed charge-transfer state is produced. The thermalization of the charge-transfer state by internal conversion places an upper limit on the time scale for charge separation in this model. As the process of internal conversion in organic materials is extremely fast, occurring within several hundred femtoseconds both in singlet[32] and triplet manifolds,[33] we assume that it will occur at a similarly fast rate in the charge-transfer manifold. Therefore, in this second mechanism, the rate of spatial separation from the hot charge-transfer state must be fast on the time scale of hundreds of femtoseconds in order for device efficiency to be appreciable.[34] This is faster than the instrument response of our experiment, and therefore we can consider that in this model the number of free (spatially separated) and bound (charge-transfer state) charges can be taken as an initial condition. The rate equations describing the second mechanism are shown in eq 2, which have the initial conditions that a fraction f of the excitons create spatially separated charges (via a hot charge-transfer state) within the pulse length of the excitation and the remaining $(1- f)$ of the excitons create charge-transfer states that decay monomolecularly. Analytic solutions can be found for the rate equations. These are shown in eq 3. The nomenclature remains as introduced for eq 1.

(24) Blom, P. W. M.; Mihailetchi, V. D.; Koster, L. J. A.; Markov, D. E. *Adv. Mater.* **2007**, *19*, 1551.
(25) Veldman, D.; Ipek, O.; Meskers, S. C. J.; Sweelssen, J.; Koetse, M. M.; Veenstra, S. C.; Kroon, J. M.; van Bavel, S. S.; Loos, J.; Janssen, R. A. J. *J. Am. Chem. Soc.* **2008**, *130*, 7721.
(26) Marsh, R. A.; Hodgkiss, J. M.; Friend, R. H. *Adv. Mater.* **2010**, *22*, 3672.
(27) Lee, J.; Vandewal, K.; Yost, S. R.; Bahlke, M. E.; Goris, L.; Baldo, M. A.; Manca, J. V.; Voorhis, T. V. *J. Am. Chem. Soc.* **2010**, *132*, 11878.
(28) Groves, C.; Marsh, R. A.; Greenham, N. C. *J. Chem. Phys.* **2008**, *129*.
(29) Inal, S.; Schubert, M.; Sellinger, A.; Neher, D. *J. Phys. Chem. Lett.* **2010**, *1*, 982.
(30) Pivrikas, A.; Juška, G.; Mozer, A. J.; Scharber, M.; Arlauskas, K.; Sariciftci, N. S.; Stubb, H.; Österbacka, R. *Phys. Rev. Lett.* **2005**, *94*, 176806.
(31) Peumans, P.; Forrest, S. R. *Chem. Phys. Lett.* **2004**, *398*, 27.
(32) Virgili, T.; Marinotto, D.; Manzoni, C.; Cerullo, G.; Lanzani, G. *Phys. Rev. Lett.* **2005**, *94*, 117402.
(33) Yang, X. D.; Lee, C. L.; Westenhoff, S.; Zhang, X. P.; Greenham, N. C. *Adv. Mater.* **2009**, *21*, 916.
(34) The term 'spatially-separated charge' is slightly misleading at high excitation intensities, as in these cases the average separation between charges can remain small due to their very high density. In this case what we mean by 'spatially-separated' charge are those charges that have lost any preferential association with their geminate pair, i.e., they are free to interact with any nearby opposite charge.

$$\begin{aligned} \mathrm{dCT}/\mathrm{d}t &= -k_{\mathrm{CT}\rightarrow\mathrm{GS}}\mathrm{CT} \\ \mathrm{dSSC}/\mathrm{d}t &= -\gamma\mathrm{SSC}^{\lambda+1} \\ \mathrm{dGS}/\mathrm{d}t &= k_{\mathrm{CT}\rightarrow\mathrm{GS}}\mathrm{CT} + \gamma\mathrm{SSC}^{\lambda+1} \end{aligned} \tag{2}$$

$$\begin{aligned} \mathrm{CT}(t) &= N_0(1-f)\exp(-k_{\mathrm{CT}\rightarrow\mathrm{GS}}t) \\ \mathrm{SSC}(t) &= (\lambda\gamma t + (fN_0)^{-\lambda})^{-1/\lambda} \\ \mathrm{GS}(t) &= N_0(1-f)(1-\exp(-k_{\mathrm{CT}\rightarrow\mathrm{GS}}t)) + \\ &\quad N_0 f - ((\lambda\gamma t + (fN_0)^{-\lambda})^{-1/\lambda} \end{aligned} \tag{3}$$

3. Results

Familiar with the possible kinetics of charge separation, and geminate and nongeminate recombination, we now examine our experimental results. In this section we first present a brief overview of how the intermolecular order and charge recombination changes through the sample series we present. We then proceed with a detailed and stepwise analysis in order to interpret the features presented in the overview, starting with RRa-P3HT, then unannealed RR-P3HT, and finally annealed RR-P3HT results. As the photophysics change with increasing P3HT order, we discuss the mechanisms for the changes and what they imply for device performance.

3.1. Effect of P3HT Order on Recombination. In Figure 2a we present the steady-state absorption spectrum of the RRa, unannealed, and annealed P3HT:PCBM blends. As expected, the absorption steadily red-shifts, due to the increased contribution to the absorption of weakly interacting H-aggregates in the regions of P3HT with high intermolecular order.[35] The intermolecular order increases from the RRa, to the unannealed and finally to the annealed RR-P3HT:PCBM blends.

Figure 2b shows the mean induced absorption from 750 to 850 nm of each sample for the first 10 ns after low intensity excitation where, as we will later confirm, monomolecular processes dominate the early time decay. We will later find that in this region, charge-transfer states and spatially separated charges have the same mean cross-section, and therefore that the transient absorption signal here is proportional to the total number of charge-transfer states plus spatially separated charge pairs. Thus, we can use this region to directly watch how the total number of charges, free and bound, changes with time. We can see that this decay changes significantly between the samples. In the RRa-P3HT:PCBM blend a large portion of the population decays within 2 ns. In the unannealed RR-P3HT:PC13M blend there is a decay component with a similar lifetime, but the weight of this component is much smaller, and consequently it results in a much smaller population loss. In the annealed RR-P3HT:PCBM blend the decay is slower, it does not exhibit the 2 ns component observed in the other two samples. Furthermore, its population loss is the least. We will find later that, at these low excitation intensities, the decay on this time scale is almost entirely monomolecular, so the amount of geminate recombination and/or monomolecular trap-assisted recombination can be approximated by the fraction of the signal that has decayed in the first 10 ns. We show these estimates of the geminate recombination losses in Figure 2c, alongside values that we extract later from a complete global model of the data. These geminate losses will directly reduce OPV performance at all light intensities, and therefore we can already hypothesize that this directly observed reduction of monomolecular recombination with increasing P3HT order is responsible for the

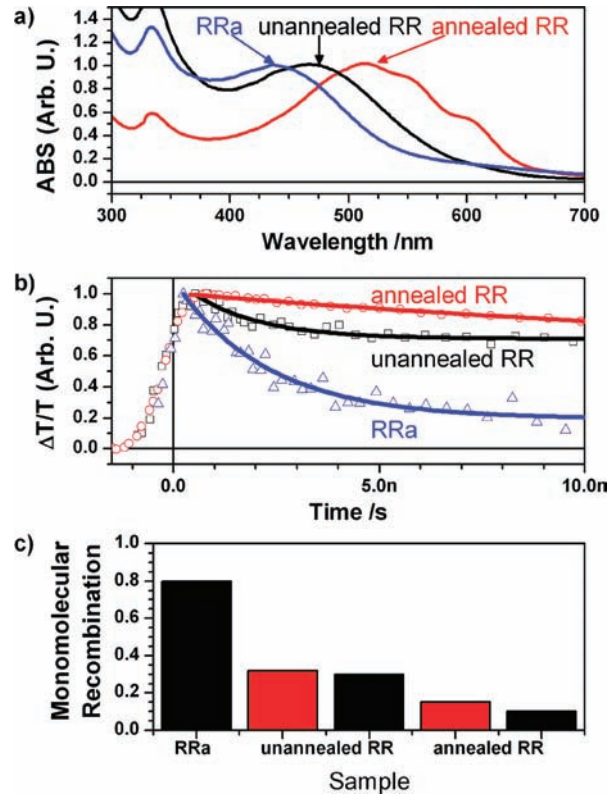

Figure 2. Comparison of RRa-P3HT:PCBM (labeled RRa), unannealed chloroform-cast RR-P3HT:PCBM (unannealed RR), and annealed chlorobenzene-cast RR-P3HT:PCBM (annealed RR) blends. Panel a shows the shift of the absorption spectra between samples due to differing interchain ordering. Panel b shows the kinetics of the charge-induced absorption over the first 10 ns at the lowest excitation intensities. The solid lines show fits to a monomolecular decay described in the text. Panel c shows the fraction of recombination that is intensity independent for each sample obtained by qualitatively examining the low-fluence decay (black bars) or from the global fit described in the text (red bars).

improvements of OPV device performance with annealing. In the following sections, we will examine this more closely and learn more about what the kinetics imply about the processes of exciton quenching, charge separation, and charge recombination. We will also discover that the effect of morphology on these processes is clearly evident in the kinetics, and that the kinetics are consistent with the development of pure P3HT ordered regions that are only on the order of a few nanometers in their most constrained dimension but much longer than this in their other dimensions.

3.2. RRa-P3HT and RRa-P3HT:PCBM. In this first subsection we start the detailed examination of the data looking at the amorphous regiorandom P3HT alone and blended 1:1 with PCBM. We find that in the pure P3HT film (no PCBM added) singlet excitons decay within 1 ns, with some fraction intersystem crossing to long-lived triplet states that decay with a lifetime of 10 μs. In contrast, we find that when PCBM is added to the blend, excitons are quenched within 100 fs and therefore no triplets are formed. The exciton quenching results predominantly in charge-transfer states which decay geminately (i.e., independent of fluence) with a characteristic inverse rate of 2 ns. This fast geminate decay explains the poor performance of amorphous P3HT:PCBM blends in solar cells.

3.2.1. Absence of Triplets in RRa-P3HT:PCBM. Recent work has demonstrated that long-lived triplet excitons are formed in

(35) Clark, J.; Silva, C.; Friend, R. H.; Spano, F. C. *Phys. Rev. Lett.* **2007**, *98*, 206406.

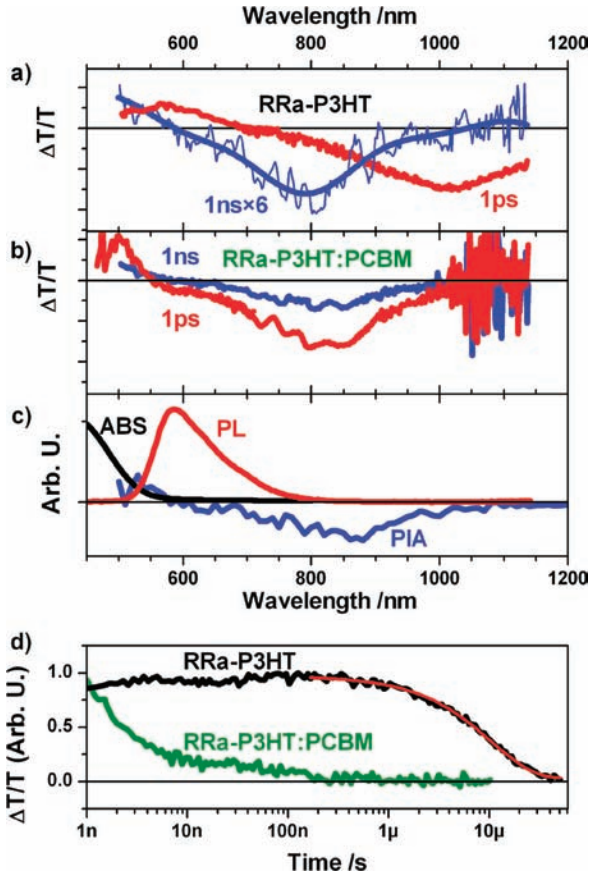

Figure 3. Panels a and b show the transient absorption spectra of regiorandom P3HT alone and blended with PCBM, respectively. The spectrum after 1 ns is multiplied by 6 for clarity in panel a. Panel c shows the absorption and photoluminescence of a RRa-P3HT film and the quasi-steady-state photoinduced absorption spectrum of a RRa-P3HT:PCBM blend (at 80 K). Panel d shows the normalized mean transient absorption of each film from 700 to 900 nm; the red line is a single exponential fit to the triplet lifetime (10 μs). The laser excitation intensity was 7 μJ/cm^2.

RRa-P3HT.[36] In order to determine the charge kinetics in a RRa-P3HT:PCBM blend, we must first ascertain whether triplet states also contribute to the observed long-lived transient absorptions in the blend. In order to do this, we compare the transient absorption of RRa-P3HT and a RRa-P3HT:PCBM blend. Figure 3a shows transient absorption spectrum of RRa-P3HT 1 ps and 1 ns after excitation (the spectrum after 1 ns is multiplied by 6 for clarity). One picosecond after photoexcitation, the excited state population is dominated by singlet excitons. The positive $\Delta T/T$ signal in the region of photoluminescence (compare red lines in Figure 3a,c) is due to stimulated emission from singlet excitons. The photoinduced absorption (negative $\Delta T/T$ signal) peaks at approximately 1000 nm, consistent with the PIA of the singlet state observed in previous work.[36] Also as found in previous work,[36] the singlet excitons decay quickly, within 1 ns, with some fraction intersystem crossing into triplet excitons which have a photoinduced absorption peaking at 800 nm (see blue line in Figure 2a). Under low fluence conditions, these triplet excitons are the dominant photoexcited state after 1 ns. The decay of these triplets is shown in Figure 3d by the black line. The red line is a fit to a monoexponential decay, from which a lifetime of 10 μs is extracted. This is slightly longer

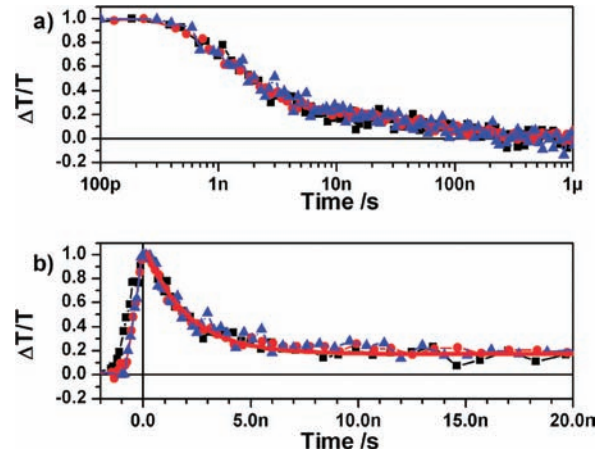

Figure 4. Panel a shows the normalized charge-induced absorption from 750−900 nm as a function of time in the RRa-P3HT:PCBM blend film after 7 (black squares), 15 (red circles), and 60 (blue triangles) μJ/cm^2 excitation pulses. Panel b shows the first 20 ns of the same data on a linear scale; the red line is a monoexponential fit yielding a geminate recombination lifetime of 2 ns.

than the lifetime of 7 μs recently reported in the literature,[36] but this discrepancy could be explained by slightly fewer triplet quenching sites (for example oxygen molecules) being present in our sample.

Figure 3b shows the transient absorption spectrum of RRa-P3HT:PCBM after 1 ps and 1 ns. No stimulated emission is observed, even at times less than 1 ps. Rather, the signal is dominated by a photoinduced absorption which is broad but peaks between 850 and 900 nm. This is the same spectrum that is observed with quasi-steady-state photoinduced absorption at low temperature (blue line in Figure 3c) and is assigned to the product of exciton quenching. This indicates that excitons are quenched much faster (in less than 100 fs) than they intersystem cross in the pristine film, and that therefore the number of triplets formed in the blend should be negligible. This is further supported by the fact that the shape of the transient spectrum in a blend does not evolve with time. Furthermore, comparing the quasi-steady-state PIA of the pristine film and the blend, the blend has an infrared absorption growing toward 2 μm typical of a charge-induced absorption, while the pristine blend does not (see Supporting Information). We therefore conclude that the products of exciton quenching dominate the excited state population of the blend, and any contribution of triplet excitons to the dynamics is exceedingly negligible.

This conclusion is supported by the dynamics presented in Figure 3d. The green line showing the induced absorption of RRa-P3HT:PCBM blend traces a much faster decay than that of the triplets observed in pristine RRa-P3HT. This clearly indicates that charges, rather than triplet excitons, dominate the excited state population in the blend and that charge recombination is faster than triplet decay.

3.2.2. Geminate Recombination in RRa-P3HT:PCBM. In order to examine how the recombination of the charges generated in RRa-P3HT:PCBM blend depends on the charge density, i.e., to investigate the roles of geminate and nongeminate processes in charge recombination, we investigate the transient absorption as a function of the excitation pulse intensity. By comparing the normalized traces of the recombination kinetics over a series of excitation intensities, the presence (or absence) of intensity-dependent recombination can be analyzed. In Figure 4a we present such a plot showing the time dependence of the

(36) Guo, J. M.; Ohkita, H.; Benten, H.; Ito, S. *J. Am. Chem. Soc.* **2009**, *131*, 16869.

normalized charge-induced absorption from 750 to 900 nm in RRa-P3HT:PCBM for a sequence of excitation pulse fluences. The decay in each case is the same, with approximately 80% of the population decaying within the first couple of nanoseconds and the remaining 20% of the population decaying on the time scale of 200 ns. This observation, that the rate of the 80% majority component of the recombination does not depend on fluence, indicates that this recombination is monomolecular and geminate. Figure 4b focuses on the major component of the recombination, showing only the first 20 ns. Fitting a single monoexponential decay to all of the curves yields the red line shown with an inverse rate for this initial geminate charge-transfer state recombination of 2 ns (rate $= 5 \times 10^8$/s). Therefore, the majority of the quenched excitons (80%) in the RRa-P3HT blend form charge-transfer states that decay within 2 ns. Previously, it has been shown that the charges bound in charge-transfer states in polymer:polymer photovoltaic blends are immobile.[12] Our observation that the charge-transfer states do not interact even at the highest excitation intensity, which corresponds to an average separation of only 3.5 nm between charge-transfer states, provides strong indirect evidence that their mobility is low. Therefore, these likely immobile, quickly decaying states are not likely to be efficiently split under the internal field of a photovoltaic cell and explain a loss mechanism of up to 80% of the absorbed photons that correlates with the poor performance of RRa-P3HT:PCBM photovoltaic devices.[37]

The inverse rate we find for geminate recombination is somewhat longer than that of 800 ps found by Ohkita et al. who measured on a 3 ns window.[7] Repeating their measurement and fitting only on a 3 ns window, we extract an inverse rate constant of 1.5 ns (see Supporting Information). This can be explained by considering there is some heterogeneity in the rate of geminate recombination, dependent on the precise interfacial alignment.[38] So although there is not complete agreement for the characteristic geminate recombination rate, we can say with certainty that it typically occurs on a time scale less than 2 ns. Finally, we ascribe the 20% of the signal that decays on a much longer time scale to nongeminate, perhaps trap-assisted, recombination of spatially separated charges.

3.3. Geminate and Nongeminate Recombination in Unannealed RR-P3HT:PCBM. With the understanding that charge recombination in the amorphous RRa-P3HT:PCBM is dominated by fast geminate recombination of charge-transfer states, we now turn to examine the photophysics of an unannealed RR-P3HT:PCBM blend. We will find that one-third of the quenched excitons produce geminate pairs that decay with the same rate as those observed in the previous section while the remaining two-thirds generate free charges, that in our test films undergo bimolecular recombination but in solar cells could be extracted.

On a time scale less than 1 ns we find that the kinetics are broadly similar to those in the RRa-P3HT:PCBM blend. Again, no stimulated emission is observed, which indicates that in the unannealed blend, exciton quenching is again essentially immediate. Hence, we begin our analysis of this blend by investigating the products of exciton quenching and their decay.

In Figure 5a we present the mean induced absorption spectrum of the unannealed RR-P3HT blend <1, then 3, and finally 100 ns after excitation. At an early time, the spectrum

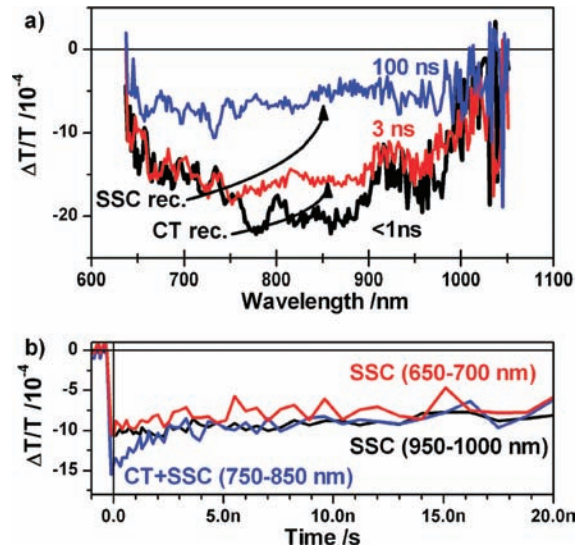

Figure 5. Panel a shows the average induced absorption spectrum of unannealed RR-P3HT:PCBM at the indicated times. CT state recombination in the first 2 ns reduces the peak at 850 nm, and then subsequent SSC recombination reduces the remaining broad induced absorption. Panel b shows the kinetics in spectral regions where the CT cross-section is much smaller than the SSC cross-section (black and red curves), and also the region where the CT state and SSC have the same mean cross-section (blue curve).

peaks at 850 nm, the peak wavelength of CT absorption observed in the previous section. We will see that this peak decays with exactly the same rate as the geminate pairs in RRa-P3HT:PCBM, leaving a broader induced absorption that decays on a time scale of hundreds of nanoseconds. Therefore, Figure 5 immediately suggests that two populations are created concurrently by exciton ionization: charge transfer states that have a peaked absorption at 850 nm and decay within 2 ns, and free charges that have a broad induced absorption and do not (at least at low to moderate fluence) decay within the first 3 ns.

In order to extract the population dynamics of charge-transfer states and spatially separated charges from the observed transient absorption signals we must know the relative cross-section of each species over the observed wavelength range. Fortunately, the analysis is greatly simplified by the observation that the CT states and SSC pairs have the same average cross-section of 5×10^{-17} cm^2 in the wavelength range 750−850 (see Supporting Information for details). In this region the transient absorption is simply proportional to the total of number charges (CT states and SSCs). Consequently, the recombination of a CT state decreases the signal by the same amount as the recombination of a SSC pair (in essence we create an artificial isosbestic 'point' by averaging a deliberately selected appropriate wavelength range). Figure 5b compares the transient absorption kinetics in regions wherein the CT cross-section is much smaller than the SSC cross-section, and therefore the transient absorption signal tracks exclusively the SSC population, with the transient absorption kinetics in the 750−850 nm region wherein the transient absorption kinetics show, with equal weighting, the kinetics of the CT states plus the kinetics of the SSC pairs. Comparing the initial value of the 750−850 nm region with the value of the plateau, we can simply estimate that one-third of the initial population are CT states while two-thirds are promptly generated free SSCs.

We now investigate the fluence dependence of the mean PIA from 750 to 850 nm in an unannealed RR-P3HT:PCBM blend.

(37) Campoy-Quiles, M.; Kanai, Y.; El-Basaty, A.; Sakai, H.; Murata, H. *Org. Electron.* **2009**, *10*, 1120.
(38) Huang, Y. S.; Westenhoff, S.; Avilov, I.; Sreearunothai, P.; Hodgkiss, J. M.; Deleener, C.; Friend, R. H.; Beljonne, D. *Nat. Mater.* **2008**, *7*, 483.

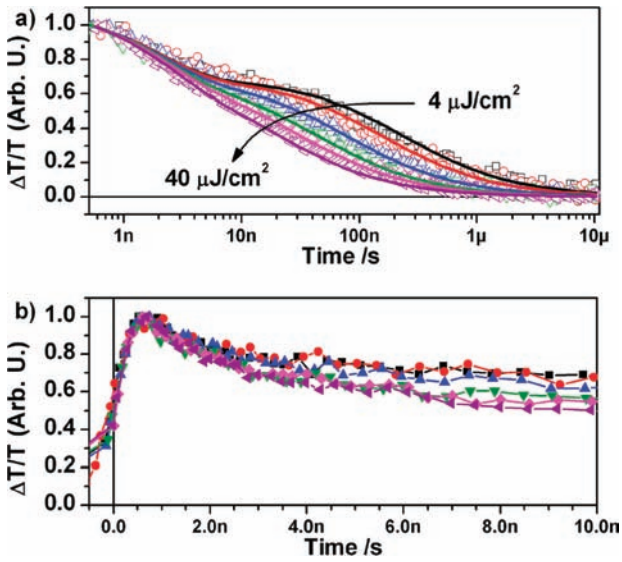

Figure 6. Panel a shows the mean induced absorption decay (750−850 nm) in an unannealed RR-P3HT:PCBM blend at various excitation intensities (open symbols), alongside global fits (solid lines) described in the text. Panel b presents the first 10 ns of the data on a linear scale to highlight the intensity independent geminate charge-transfer recombination. Excitation intensities 4, 6.5, 13, 20, 26, and 40 μJ/cm^2.

Figure 6a illustrates that in the unannealed sample a portion of the charge recombination becomes more rapid with higher intensity excitation, but also that a monomolecular, intensity-independent, component is visible that dominates the recombination in the first 2 ns. This monomolecular component is highlighted by the linear scale graph of early time shown in Figure 6b. Such mixed decay is completely consistent with our observations in Figure 5 and moreover our hypothesis that charge-transfer state recombination accounts for the decay on a time scale of less than 2 ns and that the recombination of spatially separated charges account for the remaining longer-time decay.

Let us now quantitatively consider what these observed kinetics imply about the mechanism of charge separation. Of the two mechanisms introduced in section 2, the first cannot explain a major feature of the data, namely that although the fraction of separation has substantially increased between the RRa and unannealed RR blends, the CT lifetime remains unchanged. From our observation of geminate charge-transfer state recombination in RRa-P3HT PCBM we know that $k_{CT\rightarrow GS} \approx 5 \times 10^8$/s. We observe that two-thirds of the decay in the unannealed sample is bimolecular, so two-thirds of the charge-transfer states must spatially separate. In this case $k_{CT\rightarrow GS}/(k_{CT\rightarrow SSC} + k_{CT\rightarrow GS}) = 1/3$, and therefore $k_{CT\rightarrow SSC} + k_{CT\rightarrow GS} = k_{tot} \approx 1.5 \times 10^9$/s. Therefore, for this model to be self-consistent, the CT state should decay in the unannealed RR blend in less than 1 ns. However, the CT state decay is not this fast, in fact fitting a single exponential to the early time decay results in a time constant of approximately 2 ns, unchanged from the value observed in the RRa blend. Therefore, the high yield of spatial separation is not consistent with the Onsager−Braun type model of charge generation; however, it is consistent with an ultrafast mechanism of charge generation. Given that the cross-sections of the CT and SSC are the same in the region considered, the normalized transient absorption is given by $[N_0(1 - f)\exp(-k_{CT\rightarrow GS}t) + (\lambda\gamma t + (fN_0)^{-\lambda})^{-1/\lambda}]/N_0$. Using the calculated values for N_0,(see Supporting Information) the parameters f, $k_{CT\rightarrow GS}$, λ, and γ are extracted by globally fitting the entire intensity series. Fits are performed using Origin 8 (Originlab Corporation). The data are well described by this model, as illustrated by the solid lines overlaying the data in Figure 6a). The extracted parameters along with their standard error are summarized in Table 1. To summarize, the observations of immediate bimolecular recombination and an unchanged rate of geminate recombination in the unannealed RR-P3HT:PCBM blend are inconsistent with a model of free charge formation through a charge-transfer state. They imply that quenched excitons immediately form either charge-transfer states or free charges. In the absence of field, charge-transfer states recombine geminately with the same rate as those in the amorphous RRa-P3HT:PCBM blend.

Table 1. Parameters along with Standard Error Extracted from Global Fit of Model from Section 2.3 to the Data for Unannealed RR-P3HT:PCBM and Annealed RR-P3HT:PCBM Shown in Figures 6a and 9a

parameter	unannealed	annealed
$1 - f$ (fraction monomolecular recombination)	0.32 ± 0.01	0.15 ± 0.01
f (fraction nongeminate recombination)	0.68 ± 0.01	0.85 ± 0.01
$k_{CT\rightarrow GS}$/s (geminate recombination rate)	$4.9 \pm 0.2 \times 10^8$	$2.5 \pm 0.2 \times 10^8$
$\lambda + 1$ (order of nongeminate decay)	2.18 ± 0.01	2.45 ± 0.01
γ (cm^3)$^\lambda$ s^{-1} (nongeminate decay rate)	$2.3 \pm 0.5 \times 10^{-15}$	$1.9 \pm 0.3 \times 10^{-20}$

In order to compare the recombination we observe with 3D Langevin recombination, we use the charge carrier mobility of these samples measured using the time-of-flight technique,[39] to calculate a 3D Langevin coefficient (γ_{3D}) on the order of 10^{-10} cm^{-3} s^{-1}. Then, to compare the recombination rate at specific densities between 3D Langevin recombination where $\lambda = 1$ (a pure second-order process) and extracted nongeminate recombination where $\lambda = 1.18$, we use the relation: $(dC/dt)_a/(dC/dt)_b = \gamma_a/\gamma_b C^{(\lambda_a - \lambda_b)}$. For carrier densities spanning the range from those typical in a photovoltaic device under solar illumination to the highest intensities used in this work, i.e., $10^{15}-10^{19}$/cm^3, the observed rate in the unannealed sample varies from 1/10th to 1/20th of the rate predicted by Langevin recombination. This slower-than-Langevin recombination is consistent with previous measurements[30] and has been ascribed to morphological effects decreasing the probability of charge pairs meeting.[40,41]

3.4. Nongeminate Recombination in Annealed RR-P3HT:PCBM. In this section the photophysics of the annealed P3HT:PCBM blend is studied and contrasted to the previous results. We find that a portion of the exciton quenching is no longer instantaneous, indicating that some excitons must now diffuse through regions of highly pure P3HT before encountering an interface. We also find that, unlike the less efficient amorphous and unannealed blends, there is no geminate recombination in the annealed blend. Essentially all quenched excitons immediately generate free charges even in the absence of field, explaining the high short-circuit current and fill factor of annealed P3HT:PCBM devices. The order of the recombination also changes, and although change in the carrier density dependence of the mobility and trap distributions likely plays a role in this alteration, we also raise the possibility that restricted

(39) Mauer, R.; Kastler, M.; Laquai, F. *Adv. Funct. Mater.* **2010**, *20*, 2085.
(40) Koster, L. J. A.; Mihailetchi, V. D.; Blom, P. W. M. *Appl. Phys. Lett.* **2006**, *88*, 052104.
(41) Groves, C.; Greenham, N. C. *Phys. Rev. B* **2008**, *78*, 155205.

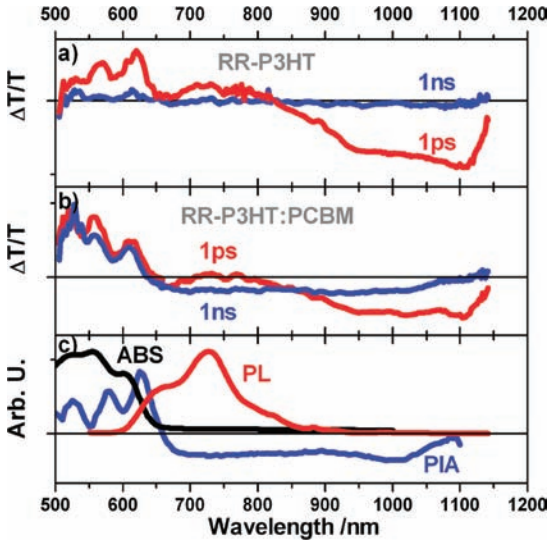

Figure 7. Panels a and b show the transient absorption spectra of regioregular P3HT alone and in an annealed blend with PCBM. Panel c shows the absorption and photoluminescence of a RR-P3HT film and the quasi-steady-state photoinduced absorption spectrum of a RR-P3HT:PCBM blend (at 80 K). The excitation fluence was ~7 μJ/cm^2.

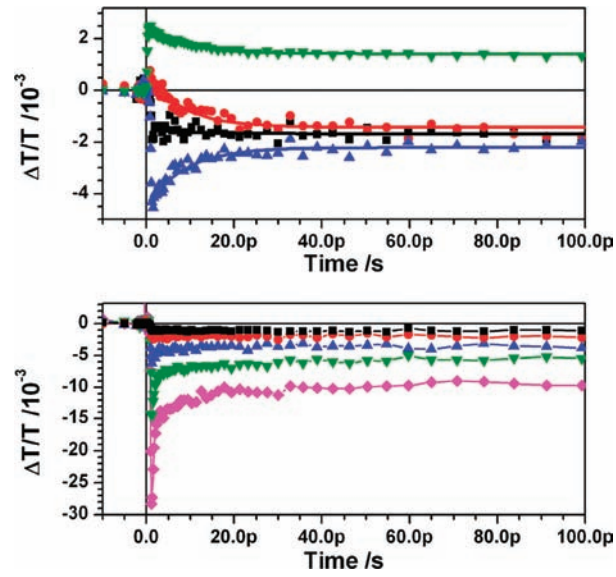

Figure 8. Panel a shows the change in transient absorption in an annealed RR-P3HT:PCBM blend over the first 100 ps for the bleach between 550 and 600 nm (green down-triangles), the region of stimulated emission between 725 and 775 nm (red circles), the isosbestic point at ~860 nm (black squares), and the region of 900−1000 nm (blue up-triangles). The solid lines show the global fit to a monoexponential decay, indicating that all the transitions are described by a 9 ps inverse rate. Panel b shows the evolution of the transient absorption at the isosbestic point after an excitation pulse with fluences of 2 (black squares), 4 (red circles), 10 (blue up-triangles), 20 (green down-triangles), and 40 μJ/cm^2 (pink diamonds). At low fluence the population remains constant over the whole time range; however, at high fluences annihilation in the first 10 ps reduces the population.

diffusion due to 2D morphological constraint of charges in the pure P3HT regions (that caused the diffusion limited exciton quenching) could be partially responsible.

3.4.1. Diffusion Limited Exciton Quenching. In the previous two samples, the exciton quenching occurred in less than 100 fs after excitation, indicating that the excitons did not need to diffuse to reach a PCBM molecule. This is not the case in the annealed blend, in which stimulated emission from excitons similar to that in pure P3HT is observed for a few picoseconds after excitation, indicating that some excitons in the annealed blend must travel significantly further in order to be quenched. Figure 7a) shows the transient absorption spectrum for pure RR-P3HT. After 1 ps (red line) the excited state population is dominated by singlet excitons. The positive $\Delta T/T$ signal in the region of the P3HT photoluminescence (red line in Figure 7c) is due to stimulated emission from the excitons. After 1 ns (blue line) the singlet excitons have decayed back into the ground state and, at the low fluences considered, the excited state population is completely diminished. Figure 7b shows the transient absorption spectrum for an annealed RR-P3HT:PCBM blend. In this case, after 1 ps (red line) the spectrum is a mixture between the exciton spectrum seen in the pure polymer and the long-lived charge signal seen in the quasi-steady-state PIA experiment (blue line in Figure 7c). The stimulated emission peaked around 720 nm is still clearly visible in the 1 ps spectrum in Figure 7b, but it is superimposed on the negative offset of charge-induced absorption from promptly generated charges. This stimulated emission in the annealed blend is a clear indication that, contrary to initial reports,[42] the exciton quenching does not occur entirely within 120 fs. This will be examined in the next section and is in agreement with recent literature.[7,43] We see that between 500 and 620 nm the absorption bleach of the singlet state is greater than the net bleach of the charge, consistent with the singlet exciton being more delocalized than the charge or the charge causing overlapping induced absorption in this region. Therefore, transition of the excited state population from singlet excitons to charges decreases the bleach in this region. In the region of the stimulated emission, from 650 to 840 nm, the induced absorption of the charges is greater than that of the exciton, and consequently the transition from exciton to charge is here accompanied by a growth in the induced absorption. In the small region roughly between 840 and 860 nm we find an isosbestic point, where the induced absorption of the singlet excitons and the charges are the same, meaning that the kinetics in this wavelength range are affected only by decay into the ground state and are unchanged by exciton quenching. Finally, we note that at longer wavelengths the induced absorption of the exciton state is greater than the induced absorption of the charge, and therefore a transition from exciton to charge is accompanied by a decrease in induced absorption. By briefly examining the kinetics in these four regions, we will determine the rate of diffusion-limited charge generation.

In Figure 8 we present the kinetics in an annealed RR-P3HT:PCBM blend on a time scale less than 100 ps. Figure 8a shows the kinetics in the region of the bleach, in the region of stimulated emission from the exciton, at the isosbestic point, and in the region of induced absorption after a low fluence excitation pulse. The black squares show the kinetics at the isosbestic point and are therefore directly proportional to the total excited state population. The invariance of the signal at the isosbestic point indicates that the total excited state population remains constant on this time scale at this low fluence. Therefore, on this time scale, there can be a conversion of excited state population from one pool to another but no recombination to the ground state. Previously, the kinetics on this time scale were ascribed to conversion of charge-transfer

(42) Hwang, I. W.; Moses, D.; Heeger, A. J. *J. Phys. Chem. C* **2008**, *112*, 4350.
(43) Marsh, R. A.; Hodgkiss, J. M.; Albert-Seifried, S.; Friend, R. H. *Nano Lett.* **2010**, *10*, 923.

states to spatially separated charges.[42] However, the continued observation of stimulated emission (red circles) unequivocally demonstrates that these dynamics involve exciton states. In order to estimate the characteristic rate with which these excitons diffuse to the interface and form charges we globally fit the kinetics to a single exponential decay. The resulting fit is shown as the solid lines in Figure 8a. An inverse rate of 9 ps is obtained, and it is clear that this single rate describes the kinetics at all regions. Therefore, these early kinetics can all be assigned to diffusion-limited exciton quenching and are comparable to those observed in polymer:polymer blends.[44] If the exciton diffusion coefficient is known, then the rate of diffusion-limited exciton quenching provides an estimate of the polymer domain size.[44] The diffusion coefficient of excitons in P3HT has recently been measured to be 1.8×10^{-3} cm^2/s,[45] from which the diffusion length in 10 ps can be calculated as $d = (Dt)^{1/2} \approx 1$ nm. Therefore, on average, excitons must only diffuse 1 nm before they are ionized in the P3HT:PCBM blend, indicating that even after annealing the smallest dimension of the pure P3HT domains is on the order of a few nanometers, allowing exciton quenching to remain very efficient.

One problem that can hinder the interpretation of transient absorption data is the emergence of second-order processes due to the high photon flux during the short excitation pulses. Figure 8b shows the kinetics at the isosbestic point for a sequence of excitation pulse fluences. At low fluence there is no change in population over the entire time range. However, starting with the 10 μJ/cm^2 fluence, a population loss in the first 10 ps starts occurring. This indicates that an annihilation mechanism starts to compete with charge-transfer at high fluences, and that therefore, at high fluences, some excitons are returned to the ground state via a second-order interaction rather than diffusing to an interface and creating charges. The most likely candidate for this interaction is exciton-charge annihilation, which has been observed to be important in similar systems.[46,47] This second-order process is observed in annealed samples because it can compete with the diffusion-limited rate of exciton quenching but not in unannealed samples because here the quenching remains faster than the second-order process (see Supporting Information). In order to assign kinetics relevant to solar cell operation, it is important to observe the transient absorption at a variety of fluences, because high fluence excitation can, as in this case, introduce second-order effects that completely mask the relevant low excitation density process.

3.4.2. Bimolecular Recombiation in Annealed P3HT:PCBM. In the previous section we observed that a portion of exciton quenching in annealed RR-P3HT is diffusion limited, indicating that highly pure regions of P3HT are formed, which have a thickness on the order of a few nanometers. In this section we find that in the annealed RR-P3HT:PCBM blend no nanosecond geminate recombination remains, indicating that free charge generation is much more efficient than in the amorphous RRa-P3HT:PCBM blend and also significantly better than in the unannealed blend. The charge-density dependence of the recombination is also altered, which is usually attributed to a change in the carrier-density dependence of the mobility or variations in the individual microstructure of devices. We observe that, in addition to these factors, a shift to more restricted diffusion in the annealed samples due to faster motion of charges in 2D ribbons could also contribute to this change in density dependence.

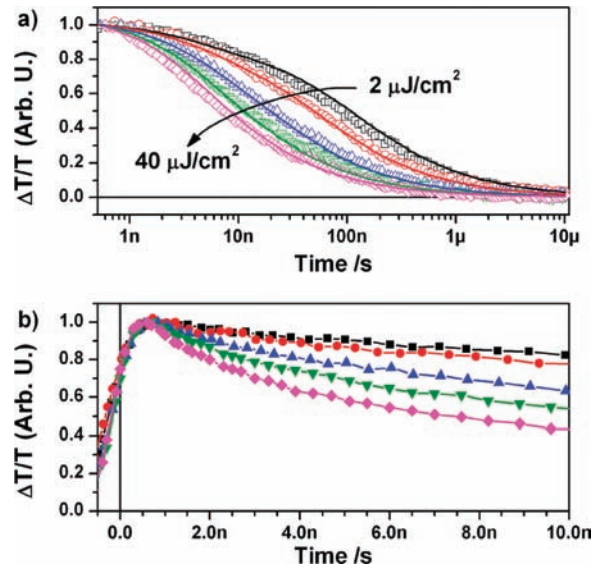

Figure 9. Panel a shows the charge induced absorption decay (750−850 nm) in an annealed RR-P3HT:PCBM blend at various excitation intensities (open symbols), alongside global fits according to mechanism 2 described in section 2 (solid lines). Panel b presents the first 10 ns of the data on a linear scale, showing that the early time decay becomes intensity independent at low intensities. Excitation intensities were 2, 4, 10, 20, and 40 μJ/cm^2.

In Figure 9a we present the fluence dependence of the mean induced absorption from 750 to 850 nm for the annealed RR-P3HT:PCBM blend. It is clearly altered from that of the unannealed blend presented in Figure 6, and on the basis of these alterations, we can make two qualitative observations. First, the absence of a clear, 2 ns, monomolecular decay component (see Figure 9b) indicates that charge-transfer state formation has been strongly suppressed by annealing, meaning that annealing has increased the generation of free carriers. Second, as Figure 9b highlights, the decay is affected by intensity from the very earliest time, even in the first nanosecond it is increased, again providing strong evidence that the generation of free carriers must happen directly following exciton quenching. Qualitatively examining Figure 9b slightly more closely, we note that at the lowest two fluences measured, which differ by a factor of 2 in pump intensity, there is little difference in the early time decay, with both signals decaying similarly to approximately 0.9 after 5 ns. This indicates that a monomolecular process is responsible for a fraction of the charge recombination at low charge densities; however, the decay is significantly slower than the charge-transfer state recombination. This suggests that, in the case of annealed P3HT:PCBM, the monomolecular charge recombination may be due to a trap or morphology-assisted process rather than geminate charge-transfer state recombination.[16,48]

In order to quantitatively examine the data, we fit it to the second mechanism for charge separation in the same way we did the unannealed data. Again, the data are well described by

(44) Westenhoff, S.; Howard, I. A.; Friend, R. H. *Phys. Rev. Lett.* **2008**, *101*, 016102.
(45) Shaw, P. E.; Ruseckas, A.; Samuel, I. D. W. *Adv. Mater.* **2008**, *20*, 3516.
(46) Howard, I. A.; Hodgkiss, J. M.; Zhang, X.; Kirov, K. R.; Bronstein, H. A.; Williams, C. K.; Friend, R. H.; Westenhoff, S.; Greenham, N. C. *J. Am. Chem. Soc.* **2010**, *132*, 328.
(47) Hodgkiss, J. M.; Tu, G. L.; Albert-Seifried, S.; Huck, W. T. S.; Friend, R. H. *J. Am. Chem. Soc.* **2009**, *131*, 8913.
(48) Tong, M. H.; Coates, N. E.; Moses, D.; Heeger, A. J.; Beaupre, S.; Leclerc, M. *Phys. Rev. B* **2010**, *81*, 125210.

the model, as illustrated by the solid lines overlaying the data in Figure 9a (the kinetics cannot be described by mechanism 1, see Supporting Information). The extracted parameters are again shown in Table 1. Comparison with the parameters extracted for the unannealed blend confirms our qualitative observations that the rate of monomolecular decay and the branching ratio between monomolecular and bimolecular recombination are changed. Fifteen percent of the charge recombination in the annealed sample is monomolecular but with a time scale twice as long as that in the unannealed and RRa blends. Given the alteration in rate, we propose this monomolecular component is not geminate charge-transfer state recombination but rather a mechanism similar to that proposed by Sundstrom and co-workers,[11] in which some charge pairs separate but are constrained by the blend morphology to stay in reasonably close proximity and recombine monomolecularly. This would indicate that roughly 15% of heterojunction sites in annealed RR-P3HT blends hinder complete spatial separation of charge and consequently lead charge pairs generated at these sites to stay close enough together that they recombine monomolecularly on a time scale under 10 ns. It is not impossible that these carriers could be separated by applied field and therefore contribute to the field dependence of the transient absorption recently observed by Friend and co-workers.[26]

The 85% majority of the free charges generated undergo density-dependent "bimolecular" recombination. However, the order of this bimolecular reaction is changed significantly, taking on a value close to 2.5 compared to that of 2.2 for the unannealed sample. Recombination in annealed RR-P3HT:PCBM solar cells with a reaction order greater than 2 has recently been correlated with a density-dependent carrier mobility,[18] which can be caused by an exponential tail of localized subgap states.[20] The order has also been observed to vary between devices[18] and has previously been found (on a longer time scale) to decrease with annealing.[16] A decrease in the reaction order after annealing is consistent with traps becoming more shallow.

On the shorter time scales we observe here, we see the opposite effect; the reaction order increased with annealing. Although carrier density dependence is likely to play a key role in determining the reaction order, and variation of the crystallinity between unannealed samples can lead to variations in the order between devices,[16] we here draw attention to the possibility that restriction of charge diffusion in 2D pure P3HT domains could contribute to an increase in reaction order with annealing. As the dimensionality of the diffusion that limits recombination is reduced, the order of the reaction is increased. For a 2D case, the reaction order expected is 2.5.[19] In the case of 2D Langevin recombination, the recombination coefficient, γ, can be calculated theoretically expressed as $\gamma_{2D} = 3\pi^{1/2}\gamma_{3D}l^{3/2}/4$, where l is the thickness of the constrained dimension.[19] With our estimate of 10^{-10} cm^{-3} s^{-1} for γ_{3D} based on TOF measurements, and the value for γ of $1.9 \pm 0.3 \times 10^{-20}$ extracted from the fit of the observed data, we can solve this expression to estimate the thickness of the constrained dimension: we obtain a value for l of 4 nm. This is consistent with the length that we previously estimated in which excitons diffuse before being quenched in the annealed film. It is also consistent with the thickness of the 2D crystalline domains recently observed using electron tomography.[6] Restriction of diffusion by the nanomorphology has previously been observed to play a key role in determining second-order interactions in polymer:polymer blends,[46] and the opportunity in this P3HT:PCBM system to couple direct experimental observation with electron tomography of the blend morphology over orders of magnitude in length scale (from the nanometer to multimicrometer) with the observation of reaction kinetics over orders of magnitude in time (from the femtosecond to multimicrosecond) offers exciting prospects to develop a fully rigorous understanding of the processes underpinning the performance of devices based on complex organic heterostructures.

4. Summary and Implications for Photovoltaic Device Performance

The key finding of our experiments in terms of photovoltaic device performance is that exciton quenching in annealed RR-P3HT:PCBM blends immediately produces free charges, even in the absence of field. This explains their high quantum efficiency and fill factor in solar cells. The ultrafast generation of free charges depends strongly on morphology. The yield of free charges is lower in unannealed blends, and very small in blends of amorphous RRa-P3HT. In these cases charge-transfer states that decay geminately within nanoseconds are also formed and will be much harder to extract in a solar cell, explaining reductions in quantum efficiency as well as fill factor. Interestingly, although the exciton energy is the highest in the RRa-P3HT and therefore the excess energy generated by exciton quenching the greatest, the free charge yield is the lowest. Therefore, contrary to suggestions that excess energy is the key criterion for free charge generation,[49] our results suggest that the ultrafast generation of free charges is more strongly related to structural order. This suggestion is consistent with results demonstrating efficient solar cells with significantly less excess energy lost at the heterojunction,[50,51] and also with recent observations that demonstrate efficient free carrier generation in annealed P3HT:PCBM devices even when an interfacial state is created without excess energy.[27]

In the unannealed blends we find 32% of quenched excitons form geminately decaying charge-transfer states. However, the IQE of unannealed devices is only around 30%,[52] which implies that the extraction of the free charges must also be rather inefficient in the unannealed blend.

In the annealed blend there is a 15% component of monomolecular decay on a time scale of ~5 ns that we attribute to spatially separated charges generated in regions of the film where further spatial separation is morphologically hindered, i.e., where one charge is trapped at or near an interface. If we assume that all exciton quenching proceeds with an inverse rate of ~10 ps and use 300 ps as the unquenched exciton lifetime (see Supporting Information), we find that 5% of excitons can decay before being quenched. Such recombination and incomplete quenching accounts for the roughly 80% IQE of annealed devices.[52] Scaled down to charge densities of 10^{16} cm^{-3}, approximately those expected in a solar cell, our results suggest the time scale for nongeminate recombination is ~3 ms. This is much longer than the charge extraction time and therefore consistent with the observation that bimolecular recombination plays little role in the device efficiency.

We therefore conclude that the key to the high efficiency of annealed P3HT:PCBM solar cells lies in their ability to directly

(49) Ohkita, H.; Cook, S.; Astuti, Y.; Duffy, W.; Tierney, S.; Zhang, W.; Heeney, M.; McCulloch, I.; Nelson, J.; Bradley, D. D. C.; Durrant, J. R. *J. Am. Chem. Soc.* **2008**, *130*, 3030.
(50) Lenes, M.; Wetzelaer, G.; Kooistra, F. B.; Veenstra, S. C.; Hummelen, J. C.; Blom, P. W. M. *Adv. Mater.* **2008**, *20*, 2116.
(51) Piliego, C.; Holcombe, T. W.; Douglas, J. D.; Woo, C. H.; Beaujuge, P. M.; Fréchet, J. M. J. *J. Am. Chem. Soc.* **2010**, *132*, 7595.
(52) Burkhard, G. F.; Hoke, E. T.; Scully, S. R.; McGehee, M. D. *Nano Lett.* **2009**, *9*, 4037.

generate free charges upon exciton quenching. This ultrafast free charge generation is strongly related to the sample morphology, with the samples with increased order showing far greater free charge generation. This can explain the morphologically dependent charge yields previously measured after longer delay times.[16,53] However, neither the role of excess energy in this process nor the exact role of ordered regions on charge generation is completely clear. Therefore, although we clearly demonstrate that fast generation of free charges is possible and underlies the high quantum efficiency and fill-factor of annealed P3HT:PCBM solar cells, the mechanism for this generation remains a question for further research.

5. Methods

Regioregular (RR) P3HT (Sepiolid P200, $M_W = 25{,}000$ g mol^{-1}, PDI = 1.6, regioregularity >98%) and regiorandom (RRa) P3HT were obtained from BASF SE. PCBM (~99%) was purchased from Aldrich. All materials were used as received. The polymers and PCBM were separately dissolved in chlorobenzene or chloroform, the solutions were mixed and then spin-cast onto precleaned quartz substrates in a nitrogen-filled glovebox. The annealed sample was heated to 120 °C for 20 min in a nitrogen-filled glovebox.

Transient absorption (TA) measurements were performed with a home-built pump−probe setup. To measure in the time range of 1−4 ns with a resolution of ~100 fs, the output of a commercial titanium:sapphire amplifier (Coherent LIBRA HE, 3.5 mJ, 1 kHz, 100 fs) was split with one portion used to generate a 532 nm excitation pulse (output of an optical parametric amplifier (Coherent OPerA Solo)) and another used to generate a white light probe using a home-built two-stage broadband (480−850 nm) noncollinear optical parametric amplifier (NOPA) for white light generation and amplification in the visible and a c-cut 3 mm thick sapphire window for white light generation in the visible to near-infrared spectral range. The variable delay of up to 4 ns between pump and probe was introduced by a broadband retroreflector mounted on a mechanical delay stage. Only reflective optics were used to guide the probe beam to the sample to minimize chirp. The excitation pulse was chopped at 500 Hz, while the white light pulses were dispersed onto a linear photodiode array which was read out at 1 kHz. Adjacent diode readings corresponding to the transmission of the sample after an excitation pulse and without an excitation pulse were used to calculate $\Delta T/T$. For measuring in the time range of 1 ns to 1 ms with a resolution of 600 ps, the excitation pulse was provided by an actively Q-switched Nd:YVO_4 laser (AOT Ltd. MOPA). The delay between pump and probe in this case was controlled by an electronic delay generator (Stanford Research Systems DG535). TA measurements were performed at room temperature under dynamic vacuum at pressures $<10^{-5}$ mbar.

Quasi-steady-state PIA experiments were performed with monochromatic light (LOT-Oriel Ommi-λ 300 monochromator) generated from a 100 W tungsten halogen light source (Müller XH 100) used as probe and the output of an UV-LED (Hamamatsu LC-L2, 365 nm) used as pump. The transmitted probe light was detected after dispersion by a second identical monochromator by an amplified silicon photodetector (Thorlabs PDA100A) in the wavelength range from 500 to 1100 nm, an InGaAs detector (Thorlabs DET10C) from 900 to 1800 nm, and a second InGaAs detector (Thorlabs DET10D) from 1800 to 2100 nm. The pump light was chopped at approximately 330 Hz by a mechanical chopper, and the change in transmission ΔT induced by the pump was extracted by using the lock-in technique (EG&G Princeton Applied Research Model 5210). Prior to the PIA measurement, the total transmission was measured to calculate $\Delta T/T$. All PIA measurements were performed in a nitrogen-cooled optical cryostat (Oxford Instruments Optistat CF) at 80 K in helium atmosphere. The total probe area was approximately 1 cm^2.

Acknowledgment. The authors thank M. Kastler (BASF SE) for kind provision of RRa-P3HT and Sepiolid P200, A. Becker for technical support, and the IRTG 1404 for funding. I.A.H. thanks the Alexander von Humboldt Foundation for a postdoctoral fellowship. F.L. thanks the Max Planck Society for funding a Max Planck Research Group. R.M. and M.M. thank the Max Planck Graduate Center (MPGC) for financial support.

Supporting Information Available: Additional PIA spectra, kinetic traces, fluence dependence, and fits to Braun−Onsager type charge generation. This information is available free of charge via the Internet at http://pubs.acs.org/.

JA105260D

(53) Keivanidis, P. E.; Clarke, T. M.; Lilliu, S.; Agostinelli, T.; Macdonald, J. E.; Durrant, J. R.; Bradley, D. D. C.; Nelson, J. *J. Phys. Chem. Lett.* **2010**, *1*, 734.